Journal of Applied Catalysis and Engineering

https://doi.org/10.17756/acce.2020-02

Research Article

Open Access

Controlling the Reduction Extent for Optimal Performance of a Ni/Al_2O_3 Dry Reforming Catalyst

Ming Li, Haoran Li, Kai Cheng, Jiazheng Ren and Yongsheng Chen*

Energy and Catalysis Laboratory, Department of Mechanical and Automation Engineering, The Chinese University of Hong Kong, Hong Kong SAR, China

***Correspondence to:**
Prof. Yongsheng Chen
Energy and Catalysis Laboratory
Department of Mechanical and Automation Engineering, The Chinese University of Hong Kong, Shatin, New Territories
Hong Kong SAR, China
Tel: (+852) 39438475
E-mail: yschen@mae.cuhk.edu.hk

Received: November 27, 2020
Accepted: December 16, 2020
Published: December 18, 2020

Citation: Li M, Li H, Cheng K, Ren J, Chen Y. 2020. Controlling the Reduction Extent for Optimal Performance of a Ni/Al_2O_3 Dry Reforming Catalyst. *J Appl Cat Chem Eng* 1(1): 2-10.

Published by United Scientific Group

Abstract

Dry reforming of methane converts two greenhouse gases (CH_4 and CO_2) into valuable syngas (H_2 and CO). Ni catalysts are commonly used for this reaction and suffer deactivation due to carbon deposition. Efforts have been devoted to improving catalyst performance including developing new catalyst formulation and synthesis methods. In this work, we started with an ordinary Ni/Al_2O_3 catalyst prepared by incipient wetness impregnation method, and carefully controlled the reduction process that activates the catalyst. With a novel control technique assisted by IR spectroscopy, we were able to well control the reduction extent in full range for the Ni catalyst. Four reduction extents (41%, 75%, 89%, and 100%) were tested for its effects on catalyst performance. It was found that 41% reduced catalyst suffered from rapid deactivation while the others performed very well with no clear sign of deactivation within 24 h of reaction time. Catalyst tests show that the performance of the 75% reduced catalyst was comparable to the top performers in the literature with CH_4 and CO_2 conversions close to the thermodynamic limit. This work would open up great opportunities for tuning catalyst performance without incurring exotic catalyst formulation and complex synthesis methods.

Keywords

Reduction extent, IR spectroscopy, Nickel catalysts, Dry reforming, Thermodynamic equilibrium

Introduction

Dry reforming of methane (DRM) has received much attention worldwide for its economic and environmental benefits as it converts two greenhouse gases (CH_4 and CO_2) into syngas (H_2 and CO) that can be used as fuels or feedstock for producing valuable chemicals as shown in equation 1 [1-5].

$$CH_4 + CO_2 \rightarrow 2CO + 2H_2, \quad \Delta H = 247.3 \text{ kJ/mol.} \qquad (1)$$

Due to its highly endothermic nature, DRM is usually carried out at high temperatures (500 - 800 °C) with the presence of a catalyst. Noble metal (Rh, Ru, Pd and Pt) based catalysts have been used for their coking resistance, high stability and activity while commercialization is hindered because of their high prices [6]. Non-noble metal (Ni, Co and Fe) based catalysts have also been investigated widely [7]. Among them Ni-based catalysts are the most commonly used due to their high activity, wide availability, and low cost [8, 9]. However, one major issue that hinders their application is the rapid deactivation caused by carbon deposition, which mainly originates from methane decomposition ($CH_4 \rightarrow 2H_2 + C$) or

Boudouard reaction ($2CO \rightarrow CO_2 + C$) [10, 11]. Extensive efforts have been devoted to improving the performance of the Ni-based catalysts. A recent review well summarizes different strategies being employed [3]. In terms of catalyst formulation, a great variety of supports have been used such as Al_2O_3, MgO, MnO, SiO_2, TiO_2, ZrO_2, CeO_2, La_2O_3, and Y_2O_3 [12-17]. Meanwhile, second catalyst components such as Pt, Rh, Ce, Mo and Co have been added to form bimetallic Ni catalysts [18-22]. Moreover, various preparation methods have also been employed to control catalyst microstructures, e.g., sol-gel [23], impregnation [24, 25], co-precipitation [26-28], polymerization [29], plasma treatment [30, 31], and atomic layer deposition [32, 33]. Specifically, promoters such as MgO and CeO_2 have also been used to control carbon deposition and hence to increase catalytic stability [27, 34].

The Ni catalysts, when prepared, are usually in an oxide form and will need to be reduced to a metallic form, upon which CH_4 adsorbs and decomposes [18, 35]. In spite of the obvious importance of defining the active catalyst component thus the catalytic properties, the reduction process is not well controlled from a scientific point of view. Reduction conditions usually include choice of reducing agent (e.g., CO, CH_4, pure H_2 gas or diluted H_2 gases) with H_2 being the most effective and commonly used [3, 36], reduction temperature (between 450 ~ 1100 °C), and reduction time that is typically in hours [3, 37, 38]. The overall observation is that the reduction process affects catalyst performance. This is no surprise because it is universally accepted that catalyst structure determines its performance. While there is no clear definition of catalyst structure, it is fair to say that overall chemical composition affects the catalyst structure and the physical properties (such as dispersion and active metal particle size) of the catalyst also play an important role [35, 39]. The existence of oxide forms of Ni before [24, 25, 37, 40, 41] during [24], and after the catalytic reaction is indicated in many works by various characterization techniques including TPR, TGA-DTA, XPS, and XANES [42, 43]. Thus, the presence of NiO after reduction is not trivial as it affects catalyst composition and inevitably the catalyst structure. This issue was well recognized as evidenced by a number of publications reporting different catalyst performance resulting from different reduction conditions [37, 40-42, 44-46]. As a result, it is difficult to conclusively determine the effect of each factor on the catalyst performance. This is a gap between the chemical and physical properties and the performance since the conditions are usually quite different. It appears that there is a lack of effective means to control the reduction extent.

Previously, we developed a technique to control the reduction extent of Ni catalyst in the full range [47]. We accomplished this by using IR spectroscopy to first obtain the reduction kinetics of the Ni catalyst through the measurement of its reduction product, water. From the kinetic measurement, we then found a quantitative relationship between the reduction time and the Ni reduction extent. In this work, we use this newly developed technique to control the reduction extent (by setting hydrogen feed time) of a 10wt%Ni/γ-Al_2O_3 and achieve optimal DRM activity, which is close to the thermodynamic limit, and excellent stability on a partially reduced catalyst.

Catalyst evaluation

Synthesis of 10wt%Ni/γ-Al_2O_3 catalyst

A 10wt.%Ni/γ-Al_2O_3 catalyst was prepared by the incipient wetness impregnation method. Typically, for every 5 g support, a precursor solution was prepared by dissolving 2.75 g $Ni(NO_3)_2 \cdot 6H_2O$ (98%, Damao Co. Ltd., Tianjin, China) in 4 ml distilled water. The precursor solution was then mixed with 5 g γ-Al_2O_3 (Hongwu Nano Co. Ltd., 99.99%) powder and stirred until uniform impregnation was achieved. After the impregnation, the sample was dried at 80 °C for 12 h. The dried sample was grounded using an agate mortar for 30 min and then calcined at 500 °C for 4 h. After calcination, the sample was grounded with an agate mortar for 30 min. Finally, the obtained sample was made in a pellet form and then crushed and sieved to a suitable size (40-60 mesh).

Catalyst evaluation

Catalytic reaction system

The dry reforming reaction was carried out in a fixed bed quartz reactor (12 mm o.d. and 8 mm i.d.) operating at atmospheric pressure. The flow rates of CH_4, CO_2 and He (internal standard) were controlled via individual mass flow controllers (Bronkhorst High-Tech B.V., the Netherlands). The reactor was held vertically, and the flow direction was downward. The catalyst was placed at the middle of the reactor on a quartz wool plug. The furnace temperature was monitored and controlled via three thermocouples located at the upper, middle, and lower zones of the furnace. All the gas lines downstream the reactor was heated at 120 °C to prevent water condensation. The reaction products were identified and their molar fractions quantified by an online FT-IR spectrometer (Nicolet iS50, Thermo Scientific, USA) and a GC (Agilent 7890B, Agilent Technologies, USA). The FT-IR spectrometer was equipped with an MCT detector. A 2-m gas cell (PIKE Technologies, Inc., USA) with a ZnSe window was placed in the beam path and maintained at 120 °C. A spectral resolution of 0.25 cm^{-1} was used, and 4 scans were averaged to generate one spectrum. These settings produced an absorbance spectrum every 0.187 min.

Catalyst reduction

Prior to each reaction, the catalyst was treated with flowing N_2 (40 ml/min at normal temperature and pressure (NTP), 1.66 mmol/min) at 750 °C to remove pre-adsorbed H_2O. Afterwards it was reduced *in situ* with a 50 mol.% H_2/N_2 flow at the same temperature and a rate of 40 ml/min (0.83 mmol/min each for H_2 and N_2). The FT-IR spectrometer was used to measure the molar fraction of the reduction product, H_2O. The reduction control technique is well described elsewhere [47]. To control the Ni reduction extent, the reduction was performed for different pre-determined periods of time, and then the 50 mol.% H_2/N_2 was switched to pure

N_2 while maintaining the same total molar flow rate. The pretreatment and reduction procedures ended until no H_2O was detected by the IR spectrometer. After finishing the reduction, the reactor was purged with flowing N_2 (40 ml/min at NTP) for 30 min while cooling down to 700 °C for DRM catalytic reaction.

DRM catalyst performance

Once the catalyst was properly reduced and the temperature reached 700 °C, CH_4 and CO_2 gases were fed into the reactor at 20.1 and 20.0 ml/min (0.835 mmol/min each for CH_4 and CO_2) at NTP to obtain equimolar CH_4 and CO_2 flows. Typically, 200 mg catalyst was used for each experiment. The gaseous hourly space velocity was 12,000 h^{-1}. The molar fractions of CH_4, CO_2, CO, and H_2O in the effluent were quantified by the IR spectrometer. 4 characteristic peaks at 3135.38 cm^{-1}, 2391.1 cm^{-1}, 2021.31 cm^{-1}, and 1966.24 cm^{-1} were selected for CH_4, CO_2, CO and H_2O, respectively. Based on the novel algorithm developed previously [48], the molar flow rates of unreacted CH_4 and CO_2, and reaction products, CO, H_2O and H_2, were calculated together with the carbon deposition rate. The conversions of CH_4 and CO_2 were calculated as equations 2 and 3,

$$X_{CH_4}(\%) = \left(1 - \frac{F_{CH_4,out}}{F_{CH_4,in}}\right) \times 100\% \quad , \qquad (2)$$

$$X_{CO_2}(\%) = \left(1 - \frac{F_{CO_2,out}}{F_{CO_2,in}}\right) \times 100\%, \qquad (3)$$

where F's stand for flow rates, and the subscripts "in" and "out" refer to influent and effluent gases, respectively.

Catalyst Characterization

X-ray Diffraction (XRD) was used to characterize the fresh and spent catalysts. The XRD patterns were collected on a Rigaku SmartLab diffractometer in the 2θ range of 10~80° at a scanning rate of 3°/min operating at 40 kV and 30 mA. Phase identification was performed by comparing the collected spectra with the JCPDS database. Ni crystallite size was estimated by using Scherrer equation after taking into account the instrument broadening measured using a standard reference material (SRM) 640b Si powder.

Results and Discussion

Controlling the reduction extent

We performed a long reduction of the 10wt.%Ni/γ-Al_2O_3 catalyst for a total of 140 minutes to establish the value of the total reducible Ni, R_0(Ni). The reduction was conducted at 750 °C under a constant flow of 50mol.% H_2/N_2. Figure 1 shows the reduction kinetics during this process. It takes about 136 min for the measured H_2O level to return to zero in the experiment. Integration of the rate over the whole reduction period gives the total amount of H_2O produced in this process, 0.335 mmol. Note that in the experiment we used 0.2 g 10 wt.%Ni/γ-Al_2O_3 catalyst so the loading of Ni was also 0.332 mmol (the value for R_0(Ni)). Thus, under the reduction conditions mentioned above, the Ni in the catalyst was completely reduced. Moreover, as shown in figure 1 the H_2 reduction has a fast kinetics at the beginning of the reaction. The measured H_2O production rate reaches a maximum value of 0.036 mmol/min at 2 min. At this rate a complete reduction could be finished within 10 min. This is surprising as hours of reduction time is commonly used in the research community.

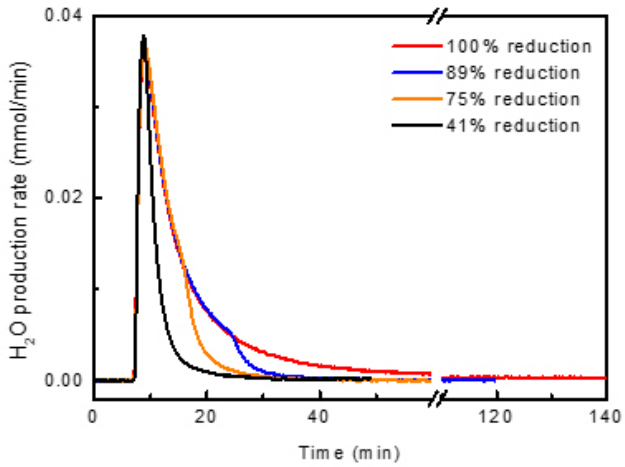

Figure 1: Hydrogen reduction kinetics for the catalyst with different reduction extents

To better understand the features of our IR-based measurement system, we also performed a short reduction of the catalyst in the same reduction conditions for 4.8 min (see SI for details).

Evidently, over 90% of the reduction takes place within the first 30 min. After 60 min, further increasing of the reduction time only results in minor increase in the catalyst reduction extent. This observation may well explain the facts that no much difference was observed when the reduction time was varied in hours [45].

To study the effect of catalyst reduction extent on its performance, we vary the reduction extent in a wide range. In addition to 100% reduction, we also attempted to produce reduction extents near 40, 70, and 90% for testing. Based on the method discussed earlier, the reduction times were set for 1.5, 8.3 and 16.9 min, respectively [47]. The measured hydrogen reduction kinetic curves for the same catalyst after these different periods of reduction are presented in figure 1. Note how well the first parts (reduction part as we discussed before) of all the partial reduction cases overlap with the full reduction kinetic curve. These curves make a sharp deviation from the full reduction kinetic curve at the exact moments when the reducing agent is turned off. Integration of a curve with regard to time gives the total amount of H_2O produced in this process, which provides the experimental value for R_t(Ni) so the real reduction extent can be calculated. Table 1 lists the predicted and real reduction extents determined from these experiments. For the first time, we demonstrate that it is probable to control the catalyst reduction extent in a wide range. The maximum difference between the experimental

measured reduction extent and the expected reduction extent is 6%, which can be substantially improved if needed.

Table 1: Comparison between the experimental and expected reduction extents.

Reduction time (min)	Predicted reduction extent (%)	Experimental reduction extent (%)
1.5	39	41
8.3	69	75
16.9	83	89

Catalyst performance

Catalyst activity

The catalyst activities of the 10wt.%Ni/γ-Al_2O_3 catalyst with different reduction extents were evaluated at 700 °C and 1 atm. This temperature was chosen because it is prone to form carbon deposition at this temperature [49], so a dramatic change can be demonstrated as a result of the controlled reduction. The reaction gas was a mixture of equimolar CH_4 and CO_2 with no dilution. The reaction for the 41% reduced catalyst only lasted for 3 h due to rapid pressure increase in the reactor. In contrast, for the 75%, 89%, and 100% reduced catalysts, the reaction was carried out for 24 h and the pressure change was minimal. The CH_4 and CO_2 conversions as well as the H_2, and CO production rates are presented in figure 2. A transient period is observed for the catalyst with all the different reduction extents. There seems to be some correlation between the consumption of certain reactant (as evidenced by its conversion kinetics) and certain product (as expressed by its production kinetics), which may shed light into the reaction mechanism for DRM. As shown in figures 2a and 2c, the kinetics for CH_4 consumption and H_2 production share quite similar features. For all (including 41% reduced) cases, the transient time is about 100 min. Meanwhile, the kinetics for CO_2 consumption and CO production are also quite similar as shown in figures 2b and 3d for all cases. Unlike CH_4 and H_2, the features are different for the 41% reduced case from other reduction conditions for CO and CO_2. The transient period for CO_2 consumption and CO production is about 200 min for 100%, 89%, and 75% reduced catalysts while no such transition is observed for the 41% case. These results seem to suggest the following regarding surface reactions involved in DRM. H_2 comes directly from CH_4 decomposition on the metal sites, which is a fast reaction and not affected much by the catalyst surface conditions; CO forms from CO_2 gasification of carbon left behind in CH_4 decomposition, which is a slower reaction and probably involves both surface oxide and metal sites.

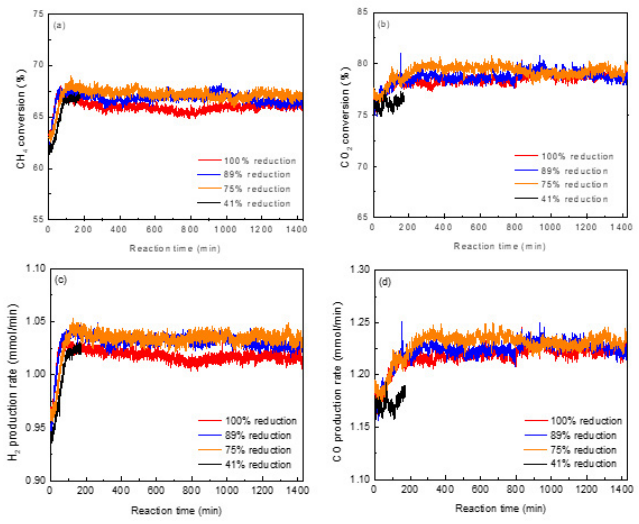

Figure 2: Conversions of (a) CH_4, (b) CO_2, as well as (c) H_2, and (d) CO production rates on the catalyst with different reduction extents. Reaction conditions: T=700 °C, P=0.1 MPa, GHSV of 12,000 ml·g-1·h-1, CH_4/CO_2=1.

Table 2 lists CH_4 and CO_2 conversions as well as H_2 and CO production rates when the reactions are fully developed. Each parameter has a similar value for all conditions even though the 41% reduced case has a much higher pressure change than the others. The biggest difference is in CO production rate, even here, the difference is less than 5% among all. Note that the H_2 production rate is lower than that of CO since some of the produced H_2 further reacts with CO_2 through reverse water gas shift (RWGS) reaction ($CO_2 + H_2 \rightarrow CO + H_2O$). It is not difficult to figure out from table 2 that about 8% of H_2 is lost in this way. Overall, the best performance is from the 75% reduced catalyst, which only takes 8.3 min to reduce. The CH_4 and CO_2 conversions are 67.5% and 79.3%, respectively.

Table 2: Catalyst activity of the 10 wt.%Ni/γ-Al_2O_3 catalyst with different reduction extents. Reaction conditions: T = 700 °C, P = 0.1 MPa, GHSV of 12, 000 ml·g^{-1}·h^{-1}, CH_4/CO_2 = 1.

Reduction extent %	X(CH_4) %	X(CO_2) %	H_2 production rate, mmol/min	CO production rate, mmol/min
41	66.8	76.3	1.02	1.18
75	67.5	79.3	1.04	1.23
89	66.8	78.8	1.04	1.23
100	66	78.5	1.02	1.22

Catalyst stability

For the 75% or higher reduced catalysts, the reaction is very stable in 24 h of reaction time as shown in figure 2. Pre- and post-reaction weight measurements give about 85 mg weight gain (see individual measurements in table S2) presumably due to carbon deposition. One advantage of the experimental setup is that it measures all gases involved including H_2O with high accuracy thus allows carbon deposition rate and H_2O production rate to be measured [48]. These two rates for all different reduction extents are shown in figure 3. The coking kinetics for the catalyst reduction conditions that allow for 24 h of testing, i.e., 75%, 89%, and 100% reduction extents, are very similar. The coking rate reaches a maximum at some point and then decreases to about 0 at around 300 min, suggesting a delicate balance between carbon formation and carbon gasification is reached at the later stage of the reaction. It is safe to say that the reaction can probably go on for much longer time without significant deactivation.

Table S1: Predicted hydrogen reduction extent of the catalyst at different reduction time.

Reduction time (min)	Predicted reduction extent (%)
0.32	5
0.46	10
0.59	15
0.72	20
1.05	30
1.26	35
1.53	40
1.92	45
2.5	50
3.37	55
4.7	60
6.47	65
8.47	70
11.07	75
14.36	80
19.13	85
26.53	90
41.53	95
136	100

Interestingly, the kinetics of H_2O production and carbon deposition are similar, suggesting possible correlation between the two reactions. As discussed before, the source of carbon formation is CH_4 decomposition, which is a fast reaction. Thus, the carbon deposition is likely to occur if the carbon gasification reaction is not fast enough to catch up. Initially, all metal surface is available for CH_4 to adsorb and decompose, thus, carbon starts to accumulate; at some point, substantial amount of the surface is covered by the carbon deposits, so CH_4 decomposition will slow down and may reach an equilibrium with the carbon gasification. CO is the product of carbon gasification. Under the reaction conditions, some CO is also produced via RWGS, producing same amount of H_2O. Therefore, the H_2O production rates in figure 3b are also the CO production rates by RWGS. The water production rate is higher for the 41% reduced catalyst when the reaction was stopped than the others having higher reduction extents in the stable operation stage; in contrast, the CO production rate is lower for the 41% reduced catalyst. Evidently, the carbon gasification rate is lower for the 41% reduced catalyst than the others. From the data, it is not difficult to estimate that the gasification rate is lowered by about 5% for the 41% reduced catalyst than the others. It is this small a difference that leads to a premature cessation of the reaction.

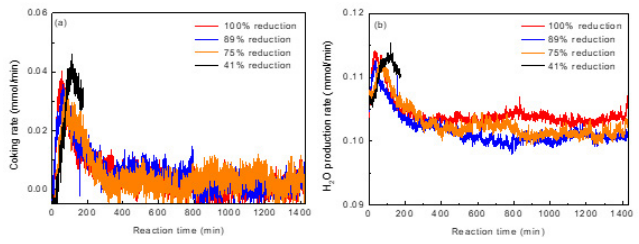

Figure 3: (a) Coking rates and **(b)** H_2O production rates on the catalyst with different reduction extents. Reaction conditions: T=700 °C, P=0.1 MPa, GHSV of 12, 000 ml·g-1·h-1, CH_4/CO_2=1.

Without proper control, many earlier works found that both physical and chemical properties varied under different pretreatment conditions and met with the difficulty to study their individual effects on the catalyst performance. In this work, there was a significant difference in the Ni reduction extent, meanwhile, these catalysts experienced same reduction temperature and reaction conditions. Post reaction XRD characterization shows that the physical properties especially the Ni particle size are almost identical among the catalysts. The XRD pattern of the fresh catalyst mainly shows the diffraction peaks of γ-Al_2O_3 (Figure S1). The XRD patterns of the spent catalysts are shown in figure 4. The spent catalysts present a typical diffraction peak of graphitic carbon at around 26°. The peak intensity is the lowest for the 41% reduced catalyst, which is consistent with the weight measurements presented in table S2. Diffraction peaks of metallic Ni are clearly present at 44.5°, 51.8° and 76.4°. The Ni crystallite sizes in the spent catalysts were estimated to be 15 nm for all the catalysts with different reduction extents. Therefore, it is reasonable to conclude that the difference of the catalyst performance is caused by the difference in the chemical composition of the catalyst, more specifically, the Ni reduction extent.

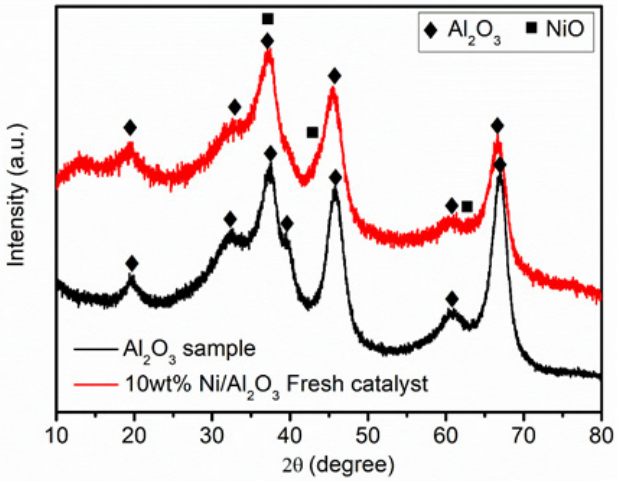

Figure S1: XRD of the γ-Al_2O_3 sample and the fresh 10 wt. %Ni/γ-Al_2O_3 catalyst.

Thermodynamic equilibrium conversions

A catalyst promotes different chemical reactions, increases reaction rates, and help reactions to reach thermodynamic equilibrium, but the thermodynamic equilibrium cannot be crossed. It is quite straightforward to compare two catalysts and judge which one is more active by comparing their conversions. It is less so to make a statement as a catalyst being active or inactive without discussing the thermodynamic limit of conversion. The driving force behind a chemical reaction is the natural tendency of the chemical system to reach lower

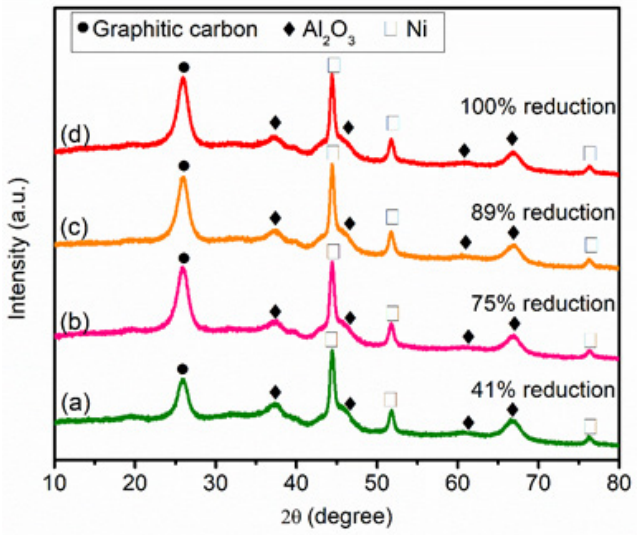

Figure 4: XRD patterns of the spent catalysts with different reduction extents.

Table S2: Experimentally measured total amounts of carbon for the catalyst with different reduction extents.

Experimental reduction extent (%)	Reaction time (h)	Weight gain (mg)	Average coking rate ($mg_{coke} \cdot g_{cat}^{-1} \cdot h^{-1}$)
41	3	45	75
75	24	84	18
89	24	96	20
100	24	76	16

total Gibbs free energy of its constituents. The total Gibbs free energy is a function of temperature, pressure, and the chemical composition of the system. The chemical composition varies with time while reactions proceed. It doesn't change randomly but is constrained by its initial composition and relevant reaction stoichiometries. Thermodynamic calculation can be performed in a few ways with Gibbs energy minimization being widely applicable and effective [50]. The difference between thermodynamic calculation and real-world reaction is clear as well as their relevance. In thermodynamic calculation, it proceeds as if there is a super catalyst that catalyzes all probable reactions to their fullest extents such that the total Gibbs free energy of the system reaches its minimum. In contrast, in a real reaction system, the catalyst usually is selective, meaning it enhances the probable reactions to different extents, and because of the limitation in reaction time and kinetics, the system usually does not reach its lowest total-Gibbs-free-energy state. Thus, the thermodynamic calculation usually predicts the highest conversion of reactants in real reactions that are similar in reaction conditions as in the calculation. For example, the calculation may not be applicable to reactions taking place in a membrane reactor in which one of the products is continuously removed, a situation that is significantly deviated from a closed system [51].

For DRM, there have been extensive thermodynamic analysis works in the literature, and several of them cover the reaction conditions used in this work, i.e., 700 °C, 1 atm, and a ratio of CH_4: CO_2=1:1 with no dilution. CH_4 and CO_2 conversions would be the same if only DRM takes place (Equation 1), however, since other reactions exist (such as RWGS which consumes extra CO_2), CH_4 and CO_2 conversions are not expected to be the same. Which conversion is higher may give hints regarding which probable reaction(s) are significant. There is, however, no consensus in this regard in the literature (Table S3). Two groups reported a CH_4 conversion at thermodynamic equilibrium at 56 or 74%, and for CO_2 conversion, 75 or 84% [50, 52]. Meanwhile, there exist six other reports having CH_4 and CO_2 conversions backwards with their values in the range of 90~92% and 65~68%, respectively [53-58]. As a matter of fact, almost

Table S3: Thermodynamic equilibrium conversions for CH_4 and CO_2 reported in the literature for DRM. Reaction conditions: T = 700 °C, P = 0.1 MPa, CH_4/CO_2 = 1 with no dilution. (These values were read from the graphs in the references and may not be absolutely accurate).

Reference[a]	CH_4 conversion (%)	CO_2 conversion (%)
Aramouni et al., [50]	56	75
Istadi et al., [52]	74	84
Nikoo et al., [53]	92	66
Chein et al., [54]	92	65
Jafarbegloo et al., [55]	90	68
Noureldin et al., [56]	90	67
Challiwala et al., [57]	91	65
Li et al., [58]	90	66

all experimental results have higher CO_2 conversion than CH_4 conversion, which is consistent with the minority findings of the thermodynamic investigations. However, to make things a little more confusing, it is not uncommon that experimental works report higher CH_4 and CO_2 conversions than what the minority findings point to [59-63]. The inconsistence most likely comes from a common practice in catalyst evaluation using gas chromatography (GC), which measures molar fractions of gases in a mixture. As pointed out in the previous work [48], it is a common mistake to calculate the CH_4 and CO_2 conversions using molar fractions measured by GC with the following equation: $X_i(\%) = (1\text{-}C_{i,out}/C_{i,in}) \cdot 100\%$, where $X_i(\%)$ is the conversion of a particular reactant, $C_{i,in}$ and $C_{i,out}$ are the influent and effluent molar fractions of the reactant [62, 64-66]. In fact, the correct way to calculate the conversion is as equation 4,

$$X_i(\%) = \left(1 - \frac{C_{i,out}}{C_{i,in}} \cdot \frac{F_{t,out}}{F_{t,in}}\right) \times 100\%, \qquad (4)$$

where $F_{t,in}$ and $F_{t,out}$ are the total molar flow rates of all gases in the influent and the effluent, respectively [47]. Since DRM is a reaction leading to an increase in the

total number of moles of the system, $F_{t,out}$ is always larger than $F_{t,in}$. Thus, using the improper equation will result in higher conversions than their real values, and the difference is not small. For example, the CH_4 and CO_2 conversions for the 75% reduced catalyst in this work are 67.5% and 79.3%, these numbers would become 81.1% and 87.9% if the improper equation were used. It is important to note that even with the improper equation, the resulting CH_4 and CO_2 conversions are in the right order, i.e., it doesn't change the fact that the CO_2 conversion is higher. Thus, almost all experimental works support the findings of the thermodynamic calculations that reported higher CO_2 conversion than CH_4 conversion. The thermodynamic equilibrium conversions for CH_4 and CO_2 reported in Aramouni's work were 56% and 75%, lower than the experimental results in this work (67.5% and 79.3% for CH_4 and CO_2 conversions, respectively) [50]. Thus, it appears that the most reasonable thermodynamic calculation that is consistent with all the experimental works is by Istadi et al., having CH_4 and CO_2 conversions of 74% and 84% at thermodynamic equilibrium [52].

Our catalyst performance after controlled reduction is comparable to the best catalysts reported in the literature. The highest CH_4 and CO_2 conversions in the literature that were properly measured is probably the $Ni@SiO_2$ work reported by Wang et al. with the initial conversions of CH_4 and CO_2 at 75% and 82%, respectively [67]. From a stability test at 750 °C, deactivation was observed for H_2 and CO yield rates within 50 h on stream. For DRM, 700 °C is a temperature more prone to carbon deposition than 750 °C. Thus, it's safe to conclude that this catalyst had a superior initial performance and significant deactivation is likely at 700 °C. Among the many works that did not mention the use of internal standard while using GC to evaluate the catalyst performance in DRM [59, 60, 62, 66, 68-70] the Ni-CaO-ZrO_2 catalyst reported by Sun *et al.* showed the highest activity with CH_4 and CO_2 conversions being around 79% and 87.5% during the stable reaction period [59]. If properly determined, these values would likely be slightly lower than the numbers we have had in the current work. No deactivation was observed for this catalyst within the 100-h test.

Conclusion

In conclusion, we have turned an ordinary Ni/Al_2O_3 catalyst into a super performer with excellent stability and high activity evidenced by CH_4 and CO_2 conversions being close to thermodynamic limit. This was made possible by scientifically controlling the reduction process that activates the catalyst leading to significantly different performance. Our control technique is robust, allowing accurate control of reduction extent in full range. In catalysis, pretreatment processes such as the reduction process are usually performed more based on individual preference or "gut feeling" rather than scientific evidence. This work provides a living example that effective monitoring and accurate controlling of these pretreatment processes will not only improve the repeatability of catalyst evaluation, but can also be an effective way of tuning catalyst performance without involving exotic catalyst formulation and difficult synthesis methods.

Acknowledgements

This work was supported by the Research Grants Council, University Grants Committee (HK) with an NSFC/RGC Joint Research Scheme Project (No. N_ CUHK 451/17), and a GRF project (No. 14307718).

Appendix A. Supplementary material

Supplementary data associated with this article are available in the online version.

References

1. Song Y, Ozdemir E, Ramesh S, Adishev A, Subramanian S, et al. 2020. Dry reforming of methane by stable Ni–Mo nanocatalysts on single-crystalline MgO. *Science* 367(6479): 777-781. http://doi.org/10.1126/science.aav2412
2. da Fonseca R, Rabelo-Neto R, Simões R, Mattos L, Noronha F. 2020. Pt supported on doped CeO_2/Al_2O_3 as catalyst for dry reforming of methane. *Int J Hydrog Energy* 45(8): 5182-5191. https://doi.org/10.1016/j.ijhydene.2019.09.207
3. Usman M, Wan Daud WMA, Abbas HF. 2015. Dry reforming of methane: influence of process parameters-a review. *Renewable Sustainable Energy Rev* 45: 710-744. https://doi.org/10.1016/j.rser.2015.02.026
4. Jang W-J, Shim J-O, Kim H-M, Yoo S-Y, Roh H-S. 2019. A review on dry reforming of methane in aspect of catalytic properties. *Catal Today* 324: 15-26. https://doi.org/10.1016/j.cattod.2018.07.032
5. Luisetto I, Tuti S, Romano C, Boaro M, Bartolomeo ED, et al. 2019. Dry reforming of methane over Ni supported on doped CeO_2: new insight on the role of dopants for CO_2 activation. *J CO_2 Util* 30: 63-78. http://doi.org/10.1016/j.jcou.2019.01.006
6. Anil C, Modak JM, Madras G. 2020. Syngas production via CO_2 reforming of methane over noble metal (Ru, Pt and Pd) doped $LaAlO_3$ perovskite catalyst. *Mol Catal* 484: 110805. https://doi.org/10.1016/j.mcat.2020.110805
7. Guerrero-Caballero J, Kane T, Haidar N, Jalowiecki-Duhamel L, Löfberg A. 2019. Ni, Co, Fe supported on Ceria and Zr doped Ceria as oxygen carriers for chemical looping dry reforming of methane. *Catal Today* 333: 251-258. http://doi.org/10.1016/j.cattod.2018.11.064
8. Aramouni NAK, Touma JG, Tarboush BA, Zeaiter J, Ahmad MN. 2018. Catalyst design for dry reforming of methane: analysis review. *Renewable Sustainable Energy Rev* 82: 2570-2585. https://doi.org/10.1016/j.rser.2017.09.076
9. Li S, Fu Y, Kong W, Pan B, Yuan C, et al. 2020. Dually confined Ni nanoparticles by room-temperature degradation of AlN for dry reforming of methane. *Appl Catal B-Environ* 277: 118921. https://doi.org/10.1016/j.apcatb.2020.118921
10. Wang S, Lu G, Millar GJ. 1996. Carbon dioxide reforming of methane to produce synthesis gas over metal-supported catalysts: State of the art. *Energy Fuels* 10(4): 896-904. https://doi.org/10.1021/ef950227t
11. Zhang Q, Zhang T, Shi Y, Zhao B, Wang M, et al. 2017. A sintering and carbon-resistant Ni-SBA-15 catalyst prepared by solid-state grinding method for dry reforming of methane. *J CO_2 Util* 17: 10-19. https://doi.org/10.1016/j.jcou.2016.11.002
12. Han JW, Park JS, Choi MS, Lee H. 2017. Uncoupling the size and support effects of Ni catalysts for dry reforming of methane. *Appl Catal B-Environ* 203: 625-632. https://doi.org/10.1016/j.apcatb.2016.10.069
13. Löfberg A, Guerrero-Caballero J, Kane T, Rubbens A, Jalowiecki-Duhamel L. 2017. Ni/CeO_2 based catalysts as oxygen vectors for the chemical looping dry reforming of methane for syngas production. *Appl Catal B-Environ* 212: 159-174. http://doi.org/10.1016/j.apcatb.2017.04.048

14. Li K, Chang X, Pei C, Li X, Chen S, et al. 2019. Ordered mesoporous Ni/La_2O_3 catalysts with interfacial synergism towards CO_2 activation in dry reforming of methane. *Appl Catal B- Environ* 259: 118092. http://doi.org/10.1016/j.apcatb.2019.118092
15. Dou J, Zhang R, Hao X, Bao Z, Wu T, et al. 2019. Sandwiched SiO_2@ Ni@ZrO_2 as a coke resistant nanocatalyst for dry reforming of methane. *Appl Catal B-Environ* 254: 612-623. http://doi.org/10.1016/j.apcatb.2019.05.021
16. Zuo Z, Liu S, Wang Z, Liu C, Huang W, et al. 2018. Dry reforming of methane on single-site Ni/MgO catalysts: Importance of site confinement. *ACS Catal* 8(10): 9821-9835. http://doi.org/10.1021/acscatal.8b02277
17. Gili A, Schlicker L, Bekheet MF, Görke O, Penner S, et al. 2018. Surface carbon as a reactive intermediate in dry reforming of methane to syngas on a 5% Ni/MnO catalyst. *ACS Catal* 8(9): 8739-8750. http://doi.org/10.1021/acscatal.8b01820
18. Egelske BT, Keels JM, Monnier JR, Regalbuto JR. 2020. An analysis of electroless deposition derived Ni-Pt catalysts for the dry reforming of methane. *J Catal* 381: 374-384. http://doi.org/10.1016/j.jcat.2019.10.035
19. Xin J, Cui H, Cheng Z, Zhou Z. 2018. Bimetallic Ni-Co/SBA-15 catalysts prepared by urea co-precipitation for dry reforming of methane. *Applied Catal A-Gen* 554: 95-104. http://doi.org/10.1016/j.apcata.2018.01.033
20. Yao L, Galvez ME, Hu C, Da Costa P. 2017. Mo-promoted Ni/Al_2O_3 catalyst for dry reforming of methane, *Int J of Hydrog Energy* 42(37): 23500-23507. http://doi.org/10.1016/j.ijhydene.2017.03.208
21. Horlyck J, Lawrey C, Lovell EC, Amal R, Scott J. 2018. Elucidating the impact of Ni and Co loading on the selectivity of bimetallic NiCo catalysts for dry reforming of methane. *Chem Eng J* 352: 572-580. http://doi.org/10.1016/j.cej.2018.07.009
22. Yan X, Hu T, Liu P, Li S, Zhao B, et al. 2019. Highly efficient and stable Ni/CeO_2-SiO_2 catalyst for dry reforming of methane: effect of interfacial structure of Ni/CeO_2 on SiO_2. *Appl Catal B-Environ* 246: 221-231. http://doi.org/10.1016/j.apcatb.2019.01.070
23. Chen C, Wang X, Zhang L, Zou X, Ding W, et al. 2017. Synthesis of mesoporous Ni-La2O_3/SiO_2 by ploy (ethylene glycol)-assisted sol-gel route as highly efficient catalysts for dry reforming of methane with a H_2/CO ratio of unity. *Catal Commun* 94: 38-41. http://doi.org/10.1016/j.catcom.2017.02.018
24. Margossian T, Larmier K, Kim SM, Krumeich F, Fedorov A, et al. 2017. Molecularly tailored nickel precursor and support yield a stable methane dry reforming catalyst with superior metal utilization. *J Am Chem Soc* 139(20): 6919-6927. http://doi.org/10.1021/jacs.7b01625
25. Theofanidis SA, Galvita VV, Poelman H, Dharanipragada NVRA, Longo A, et al. 2018. Fe-containing magnesium aluminate support for stability and carbon control during methane reforming. *ACS Catal* 8(7): 5983-5995. http://doi.org/10.1021/acscatal.8b01039
26. Wolfbeisser A, Sophiphun O, Bernardi J, Wittayakun J, Fottinger K, et al. 2016. Methane dry reforming over ceria-zirconia supported Ni catalysts. *Catal Today* 277: 234-245. http://doi.org/10.1016/j.cattod.2016.04.025
27. Mette K, Kühl S, Tarasov A, Willinger MG, Kröhnert J, et al. 2016. High-temperature stable Ni nanoparticles for the dry reforming of methane. *ACS Catal* 6(10): 7238-7248. http://doi.org/10.1021/acscatal.6b01683
28. Guo Y, Lu J, Liu Q, Bai X, Gao L, et al. 2018. Carbon dioxide reforming of methane over cobalt catalysts supported on hydrotalcite and metal oxides. *Catal Commun* 116: 81-84. http://doi.org/10.1016/j.catcom.2018.08.017
29. Silva CKS, Baston EP, Melgar LZ, Bellido JDA. 2019. Ni/Al_2O_3-La_2O_3 catalysts synthesized by a one-step polymerization method applied to the dry reforming of methane: effect of precursor structures of nickel, perovskite and spinel. *React Kinet Mech Catal* 128: 251-269. http://doi.org/10.1007/s11144-019-01644-3
30. Sheng Z, Kim HH, Yao S, Nozaki T. 2020. Plasma-chemical promotion of catalysis for CH_4 dry reforming: unveiling plasma-enabled reaction mechanisms. *Phys Chem Chem Phys* 22 (34): 19349-19358. https://doi.org/10.1039/d0cp03127e
31. Hu X, Jia X, Zhang X, Liu Y, Liu CJ. 2019. Improvement in the activity of Ni/ZrO_2 by cold plasma decomposition for dry reforming of methane. *Catal Commun* 128: 105720. http://doi.org/10.1016/j.catcom.2019.105720
32. Gould TD, Izar A, Weimer AW, Falconer JL, Medlin JW. 2014. Stabilizing Ni catalysts by molecular layer deposition for harsh, dry reforming conditions. *ACS Catal* 4(8): 2714-2717. http://doi.org/10.1021/cs500809w
33. Lin C, Jang JB, Zhang L, Stach EA, Gorte RJ. 2018. Improved coking resistance of "Intelligent" Ni catalysts prepared by atomic layer deposition. *ACS Catal* 8(8): 7679-7687. http://doi.org/10.1021/acscatal.8b01598
34. Chen W, Zhao G, Xue Q, Chen L, Lu Y. 2013. High carbon-resistance $Ni/CeAlO_3$-Al_2O_3 catalyst for CH_4/CO_2 reforming. *Appl Cataly B-Environ* 136-137: 260-268. http://doi.org/10.1016/j.apcatb.2013.01.044
35. Kawi S, Kathiraser Y, Ni J, Oemar U, Li Z, et al. 2015. Progress in synthesis of highly active and stable nickel-based catalysts for carbon dioxide reforming of methane. *ChemSusChem* 8(21): 3556-3575. http://doi.org/10.1002/cssc.201500390
36. Gao Y, Jiang J, Meng Y, Yan F, Aihemaiti A. 2018. A review of recent developments in hydrogen production *via* biogas dry reforming. *Energy Convers Manage* 171: 133-155. http://doi.org/10.1016/j.enconman.2018.05.083
37. Pino L, Italiano C, Vita A, Laganà M, Recupero V. 2017. $Ce_{0.70}La_{0.20}Ni_{0.10}O_{2-\delta}$ catalyst for methane dry reforming: influence of reduction temperature on the catalytic activity and stability. *Appl Catal B-Environ* 218: 779-792. http://doi.org/10.1016/j.apcatb.2017.06.080
38. Erdogan B, Arbag H, Yasyerli N. 2018. SBA-15 supported mesoporous Ni and Co catalysts with high coke resistance for dry reforming of methane. *Int J Hydrog Energy* 43: 1396-1405. http://doi.org/10.1016/j.ijhydene.2017.11.127
39. Abdullah B, Ghani NAA, Vo D-VN. 2017. Recent advances in dry reforming of methane over Ni-based catalysts. *J Clean Prod* 162: 170-185. http://doi.org/10.1016/ j.jclepro.2017.05.176
40. Zhou L, Li L, Wei N, Li J, Basset J-M. 2015. Effect of $NiAl_2O_4$ Formation on Ni/Al_2O_3 stability during dry reforming of methane, *ChemCatChem* 7(16): 2508-2516. http://doi.org/10.1002/cctc.201500379
41. Chai Y, Fu Y, Feng H, Kong W, Yuan C, et al. 2018. A nickel-based perovskite catalyst with a bimodal size distribution of nickel particles for dry reforming of methane. *ChemCatChem* 10(9): 2078-2086. http://doi.org/10.1002/cctc.201701483
42. Juan-Juan J, Román-Martínez MC, Illán-Gómez MJ. 2009. Nickel catalyst activation in the carbon dioxide reforming of methane: effect of pretreatments. *Appl Catal A-Gen* 355(1-2): 27-32. http://doi.org/10.1016/j.apcata.2008.10.058
43. Rogers JL, Mangarella MC, D'Amico AD, Gallagher JR, Dutzer MR, et al. 2016. Differences in the nature of active sites for methane dry reforming and methane steam reforming over nickel aluminate catalysts. *ACS Catal* 6(9): 5873-5886. http://doi.org/10.1021/acscatal.6b01133
44. Al-Fatesh ASA, Fakeeha AH. 2012. Effects of calcination and activation temperature on dry reforming catalysts. *J Saudi Chem Soc* 16(1): 55-61. http://doi.org/10.1016/j.jscs.2010.10.020
45. Kim SS, Choi HJ, Hong SC. 2012. Effect of pretreatment time in dry reforming over Ni/TiO_2 catalyst. *J Chem Eng Japan* 45(1): 41-45. http://doi.org/10.1252/jcej.11we080
46. Schwengber CA, da Silva FA, Schaffner RA, Fernandes-Machado NRC, Ferracin RJ, et al. 2016. Methane dry reforming using Ni/

Al_2O_3 catalysts: evaluation of the effects of temperature, space velocity and reaction time. *J Environ Chem Eng* 4(3): 3688-3695. http://doi.org/10.1016/j.jece.2016.07.001

47. Li M, Cheng K, Ren J, Chen Y. 2019. Controlling the reduction extent for metal catalysts. *ChemistrySelect* 4(19): 5496-5502. http://doi.org/10.1002/slct.201901210
48. Ren J, Lee AC, Cheng K, Li M, Chen Y. 2018. Measuring the unmeasurable by IR spectroscopy: carbon deposition kinetics in dry reforming of methane. *ChemPhysChem* 19(15): 1814-1819. http://doi.org/10.1002/cphc.201800137
49. Arora S, Prasad R. 2016. An overview on dry reforming of methane: strategies to reduce carbonaceous deactivation of catalysts. *RSC Adv* 6(110): 108668-108688. https://doi.org/10.1039/c6ra20450c
50. Aramouni NAK, Zeaiter J, Kwapinski W, Ahmad MN. 2017. Thermodynamic analysis of methane dry reforming: Effect of the catalyst particle size on carbon formation. *Energy Convers Manage* 150: 614-622. http://doi.org/10.1016/j.enconman.2017.08.056
51. Sumrunronnasak S, Tantayanon S, Kiatgamolchai S, Sukonket T. 2016. Improved hydrogen production from dry reforming reaction using a catalytic packed-bed membrane reactor with Ni-based catalyst and dense PdAgCu alloy membrane. *Int J Hydrog Energy* 41(4): 2621-2630. http://doi.org/10.1016/j.ijhydene.2015.10.129
52. Istadi I, Amin NAS. 2005. Co-generation of C2 hydrocarbons and synthesis gases from methane and carbon dioxide: a thermodynamic analysis. *J Nat Gas Chem* 13(3): 148-159.
53. Nikoo MK, Amin NAS. 2011. Thermodynamic analysis of carbon dioxide reforming of methane in view of solid carbon formation. *Fuel Process Technol* 92(3): 678-691. http://doi.org/10.1016/j.fuproc.2010.11.027
54. Chein RY, Chen YC, Yu CT, Chung JN. 2015. Thermodynamic analysis of dry reforming of CH_4 with CO_2 at high pressures. *J Nat Gas Sci Eng* 26: 617-629. http://doi.org/10.1016/j.jngse.2015.07.001
55. Jafarbegloo M, Tarlani A, Mesbah AW, Sahebdelfar S. 2015. Thermodynamic analysis of carbon dioxide reforming of methane and its practical relevance. *Int J Hydrogen Energy* 40(6): 2445-2451. http://doi.org/10.1016/j.ijhydene.2014.12.103
56. Noureldin MMB, Elbashir NO, El-Halwagi MM. 2014. Optimization and selection of reforming approaches for syngas generation from natural/shale gas. *Ind Eng Chem Res* 53(5): 1841-1855. http://doi.org/10.1021/ie402382w
57. Challiwala MS, Ghouri MM, Linke P, El-Halwagi MM, Elbashir NO. 2017. A combined thermo-kinetic analysis of various methane reforming technologies: comparison with dry reforming. *J CO_2 Util* 17: 99-111. http://doi.org/10.1016/j.jcou.2016.11.008
58. Li Y, Wang Y, Zhang X, Mi Z. 2008. Thermodynamic analysis of autothermal steam and CO_2 reforming of methane. *Int J Hydrog Energy* 33(10): 2507-2514. http://doi.org/10.1016/j.ijhydene.2008.02.051
59. Sun N, Wen X, Wang F, Wei W, Sun Y. 2010. Effect of pore structure on Ni catalyst for CO_2 reforming of CH_4. *Energy Environ Sci* 3(3): 366-369. https://doi.org/10.1039/b925503f
60. Wang S, Lu GQ. 1998. Role of CeO_2 in Ni/CeO_2-Al_2O_3 catalysts for carbon dioxide reforming of methane. *Appl Catal B-Environ* 19(3-4): 267-277. http://doi.org/10.1016/S0926-3373(98)00081-2
61. Zhang X, Zhang Q, Tsubaki N, Tan Y, Han Y. 2015. Carbon dioxide reforming of methane over Ni nanoparticles incorporated into mesoporous amorphous ZrO_2 matrix. *Fuel* 147: 243-252. http://doi.org/10.1016/j.fuel.2015.01.076
62. Frontera P, Macario A, Aloise A, Antonucci PL, Giordano G, et al. 2013. Effect of support surface on methane dry-reforming catalyst preparation. *Catal Today* 218: 18-29. http://doi.org/10.1016/j.cattod.2013.04.029
63. Özkara-Aydınoğlu S, Özensoy E, Aksoylu AE. 2009. The effect of impregnation strategy on methane dry reforming activity of Ce promoted Pt/ZrO_2. *Int J Hydrog Energy* 34(24): 9711-9722. http://doi.org/10.1016/j.ijhydene.2009.09.005
64. Damyanova S, Pawelec B, Palcheva R, Karakirova Y, Sanchez MCC, et al. 2018. Structure and surface properties of ceria-modified Ni-based catalysts for hydrogen production. *Appl Catal B-Environ* 225: 340-353. http://doi.org/10.1016/j.apcatb.2017.12.002
65. Rahemi N, Haghighi M, Babaluo AA, Jafari MF, Estifaee P. 2013. CO_2 reforming of CH_4 over CeO_2-doped Ni/Al_2O_3 nanocatalyst treated by non-thermal plasma. *J. Nanosci Nanotechnol* 13(7): 4896-4908. http://doi.org/10.1166/jnn.2013.7585
66. Al-Fatesh A. 2015. Suppression of carbon formation in CH_4-CO_2 reforming by addition of Sr into bimetallic Ni-Co/γ-Al_2O_3 catalyst. *J King Saud Univ Eng Sci* 27(1): 101-107. http://doi.org/10.1016/j.jksues.2013.09.006
67. Wang F, Han B, Zhang L, Xu L, Yu H, et al. 2018. CO_2 reforming with methane over small-sized $Ni@SiO_2$ catalysts with unique features of sintering-free and low carbon. *Appl Catal B-Environ* 235: 26-35. http://doi.org/10.1016/j.apcatb.2018.04.069
68. Kathiraser Y, Thitsartarn W, Sutthiumporn K, Kawi S. 2013. Inverse $NiAl_2O_4$ on $LaAlO_3$-Al2O_3: unique catalytic structure for stable CO_2 reforming of methane. *J Phys Chem C* 117(16): 8120-8130. http://doi.org/ 10.1021/jp401855x
69. Paksoy AI, Caglayan BS, Aksoylu AE. 2015. A study on characterization and methane dry reforming performance of Co-Ce/ZrO_2 catalyst. *Appl Catal B-Environ* 168-169: 164-174. http://doi.org/10.1016/j.apcatb.2014.12.038
70. Shamskar FR, Rezaei M, Meshkani F. 2017. The influence of Ni loading on the activity and coke formation of ultrasound-assisted co-precipitated Ni-Al_2O_3 nanocatalyst in dry reforming of methane. *Int J Hydrogen Energy* 42(7): 4155-4164. http://doi.org/10.1016/j.ijhydene.2016.11.067